

# Computational Science Laboratory

## Report CSL-TR-20-6

June 2, 2022

Steven Roberts, Andrey A Popov, Arash  
Sarshar, and Adrian Sandu

*“A fast time-stepping strategy for  
dynamical systems equipped with a  
surrogate model”*

Computational Science Laboratory  
“Compute the Future!”

Department of Computer Science  
Virginia Polytechnic Institute and State University  
Blacksburg, VA 24060  
Phone: (540)-231-2193  
Fax: (540)-231-6075  
Email: [steven94@vt.edu](mailto:steven94@vt.edu), [apopov@vt.edu](mailto:apopov@vt.edu), [sarshar@vt.edu](mailto:sarshar@vt.edu),  
[sandu@cs.vt.edu](mailto:sandu@cs.vt.edu)  
Web: <http://csl.cs.vt.edu>



# A FAST TIME-STEPPING STRATEGY FOR DYNAMICAL SYSTEMS EQUIPPED WITH A SURROGATE MODEL\*

STEVEN ROBERTS<sup>†</sup>, ANDREY A POPOV<sup>†</sup>, ARASH SARSHAR<sup>†</sup>, AND ADRIAN SANDU<sup>†</sup>

**Abstract.** Simulation of complex dynamical systems arising in many applications is computationally challenging due to their size and complexity. Model order reduction, machine learning, and other types of surrogate modeling techniques offer cheaper and simpler ways to describe the dynamics of these systems, but are inexact and introduce additional approximation errors. In order to overcome the computational difficulties of the full complex models, on one hand, and the limitations of surrogate models, on the other, this work proposes a new accelerated time-stepping strategy that combines information from both. This approach is based on the multirate infinitesimal general-structure additive Runge–Kutta (MRI-GARK) framework. The inexpensive surrogate model is integrated with a small timestep to guide the solution trajectory, and the full model is treated with a large timestep to occasionally correct for the surrogate model error and ensure convergence. We provide a theoretical error analysis, and several numerical experiments, to show that this approach can be significantly more efficient than using only the full or only the surrogate model for the integration.

**Key words.** Multirate time integration, Surrogate model, General-structure additive Runge–Kutta methods, Reduced-order modeling, Machine learning

**AMS subject classifications.** 65L05, 65F99

**1. Introduction.** This paper will consider the system of ordinary differential equations (ODEs)

$$(1.1) \quad y' = f(t, y), \quad y(t_0) = y_0, \quad y \in \mathbb{C}^N,$$

equipped with a surrogate model approximating the dynamics of (1.1):

$$(1.2) \quad y'_{\text{sur}} = f_{\text{sur}}(t, y_{\text{sur}}), \quad y_{\text{sur}} \in \mathbb{C}^S.$$

This surrogate model is assumed to be much less expensive to solve than the full model (1.1), possibly by evolving in a lower dimensional space ( $S < N$ ). Moreover, we assume that projections between the full and surrogate model spaces are realized by the matrices  $\mathbf{V}, \mathbf{W} \in \mathbb{C}^{N \times S}$ :

$$(1.3) \quad y_{\text{sur}} = \mathbf{W}^* y, \quad y \approx \mathbf{V} y_{\text{sur}}, \quad \mathbf{W}^* \mathbf{V} = \mathbf{I}_{S \times S}.$$

Here, the “\*” symbol denotes the conjugate transpose of a matrix.

This paper presents a new technique to supplement the numerical integration of (1.1) using the surrogate model (1.2). For an appropriate choice of surrogate model, our method can be significantly more efficient than using either the full or the surrogate model alone. This is accomplished by applying a multirate time integration scheme to the following ODE with fast dynamics  $f^{\{\text{f}\}}$  and slow dynamics  $f^{\{\text{s}\}}$ :

$$(1.4) \quad y' = \underbrace{\mathbf{V} f_{\text{sur}}(t, \mathbf{W}^* y)}_{f^{\{\text{f}\}}(t, y)} + \underbrace{f(t, y) - \mathbf{V} f_{\text{sur}}(t, \mathbf{W}^* y)}_{f^{\{\text{s}\}}(t, y)}.$$

---

\*Submitted to the editors DATE.

**Funding:** This work was supported by awards NSF ACI-1709727, NSF CDS&E-MSS 1953113, DE-SC0021313, and by the Computational Science Laboratory at Virginia Tech.

<sup>†</sup>Computational Science Laboratory, Virginia Polytechnic Institute and State University, Blacksburg, VA 24060 ([steven94@vt.edu](mailto:steven94@vt.edu), [apopov@vt.edu](mailto:apopov@vt.edu), [sarshar@vt.edu](mailto:sarshar@vt.edu), [sandu@cs.vt.edu](mailto:sandu@cs.vt.edu)).

Multirate methods are characterized by using different stepsizes for different parts of an ODE, as opposed to a single, global timestep [3, 11, 12, 18, 19, 21, 37, 43, 44]. For problems with partitions exhibiting vastly different time scales, stiffnesses, evaluation costs, or amounts of nonlinearity, multirate methods can be more efficient than their single rate counterparts. In (1.4), the fast partition  $f^{\{f\}}$  is treated with a small timestep, and the slow partition  $f^{\{s\}}$  is treated with a large timestep. Note that (1.4) has the same solution as (1.1). It is rewritten and partitioned, however, in such a way that  $f^{\{f\}}$  contains the surrogate model dynamics and  $f^{\{s\}}$  represents the error in the surrogate model. Ideally, this error will be small, so a large timestep would be acceptable. Moreover, this means expensive evaluations of the full model occur infrequently compared to the inexpensive surrogate model evaluations.

With about 60 years of development [37], the multirating strategy has been applied to numerous classes of time integration methods. Conceivably any multirate method suitable for additively partitioned systems could be applied to (1.4). This paper builds upon multirate infinitesimal methods [6, 25, 45, 47, 51], as they offer a particularly flexible and elegant approach to multirate integration. In particular, we use the multirate infinitesimal general-structure additive Runge–Kutta (MRI-GARK) framework proposed in [39, 42]. MRI-GARK is an appealing choice as it generalizes many types of multirate infinitesimal methods, allows for the construction of high order methods, and supports implicit stages. We note, however, that this paper primarily focuses on explicit methods where (1.1) is nonstiff.

There are other instances in the literature where multirate methods and surrogate models are used in conjunction. In [22], an implicit multirate scheme is used to simulate a fast-evolving electric circuit coupled with a slow-evolving electric field. Model order reduction is then applied to the electric field problem to further reduce the computational cost. A multirate Runge–Kutta–Chebyshev method is proposed in [1] using a time-averaged right-hand side, which can be viewed as a surrogate model with better stiffness properties. Also related are high-order/low-order (HOLO) methods [9] for systems of nonlinear equations where a high-complexity model is coupled with a low-complexity model. HOLO is based on nonlinear elimination [26], and has the computationally appealing property that nonlinear solves are performed in a low-dimensional space. Finally, surrogate models have been used extensively to speed up optimization problems when objective function evaluations are expensive [14, 30, 33].

This remainder of this paper is structured as follows. In section 2, we review the MRI-GARK framework and extensions. Section 3 then specializes MRI-GARK-type methods to the special ODE (1.4). An error analysis is performed in section 4, and various approaches for constructing surrogate models are discussed in section 5. Convergence and performance experiments can be found in section 6. Finally, section 7 summarizes the results of the paper and proposes future extensions.

**2. Multirate infinitesimal general-structure additive Runge–Kutta methods.** In this section, we will briefly review the MRI-GARK framework, as it serves as the foundation for the remainder of the paper. These methods numerically solve ODEs that are additively partitioned into fast and slow dynamics:

$$(2.1) \quad y' = f^{\{f\}}(y) + f^{\{s\}}(y).$$

The defining characteristic of multirate infinitesimal methods is that the slow dynamics  $f^{\{s\}}$  is propagated with a discrete method, most commonly a Runge–Kutta method, while the fast dynamics  $f^{\{f\}}$  is propagated continuously through modified fast ODEs. An MRI-GARK scheme [42] advances the solution of (2.1) from time  $t_n$

to  $t_{n+1} = t_n + H$  via the following computational process:

$$\begin{aligned}
 (2.2a) \quad & Y_1^{\{s\}} = y_n, \\
 (2.2b) \quad & \begin{cases} v_i(0) = Y_i^{\{s\}}, \\ T_i = t_n + c_i^{\{s\}} H, \\ v'_i(\theta) = \Delta c_i^{\{s\}} f^{\{f\}}(T_i + \Delta c_i^{\{s\}} \theta, v_i(\theta)) + \sum_{j=1}^{i+1} \gamma_{i,j} \left(\frac{\theta}{H}\right) f^{\{s\}}(T_j, Y_j^{\{s\}}), \\ \text{for } \theta \in [0, H], \\ Y_{i+1}^{\{s\}} = v_i(H), \quad i = 1, \dots, s^{\{s\}}, \end{cases} \\
 (2.2c) \quad & y_{n+1} = Y_{s^{\{s\}}+1}^{\{s\}}.
 \end{aligned}$$

There are  $s^{\{s\}}$  modified fast ODEs (2.2b) solved between the abscissae of a Runge–Kutta method. The distances between consecutive abscissae are

$$\Delta c_i^{\{s\}} = \begin{cases} c_{i+1}^{\{s\}} - c_i^{\{s\}}, & i = 1, \dots, s^{\{s\}} - 1, \\ 1 - c_{s^{\{s\}}}^{\{s\}}, & i = s^{\{s\}}. \end{cases}$$

Equation (2.2b) also contains time-dependent, polynomial forcing terms for the slow dynamics which satisfy

$$(2.3) \quad \gamma_{i,j}(t) := \sum_{k \geq 0} \gamma_{i,j}^k t^k, \quad \tilde{\gamma}_{i,j}(t) := \int_0^t \gamma_{i,j}(\tau) d\tau = \sum_{k \geq 0} \gamma_{i,j}^k \frac{t^{k+1}}{k+1}, \quad \bar{\gamma}_{i,j} := \tilde{\gamma}_{i,j}(1).$$

Continuing with the notation of [42], capitalized versions of (2.3) denote matrices of coefficients. If  $\bar{\Gamma}$  is lower triangular, (2.2) is explicit, and otherwise, it is implicit.

For general  $f^{\{f\}}$  one cannot expect to find a closed-form solution to the modified fast ODE (2.2b); however by time-stepping it with an “infinitesimally” small timestep, one can determine  $v_i(H)$  exactly. For purposes of computational practicality, the infinitesimally small timestep is loosened to a timestep small enough that fast solution errors are negligible. Multirate infinitesimal methods enjoy great flexibility in that *any* consistent time integration method can be used to solve the modified fast ODE provided sufficiently many steps are taken. This offers the freedom to choose implicit or explicit methods, as well as methods of any order. Equation (2.2) is multirate in the sense that there are  $s^{\{s\}}$  evaluations of  $f^{\{s\}}$  over a timestep  $H$ , while (2.2b) is generally integrated with a much smaller timestep and requires many more evaluations of  $f^{\{f\}}$ .

**2.1. Coupled MRI-GARK schemes.** In [39] two new types of MRI-GARK methods were proposed: step predictor-corrector MRI-GARK (SPC-MRI-GARK) and internal predictor-corrector MRI-GARK (IPC-MRI-GARK). In order to improve the linear stability of MRI-GARK, both include coupled, discrete prediction stages that are subsequently corrected by solving modified fast ODEs. In comparing the two MRI-GARK variants, SPC-MRI-GARK was identified to have simpler order conditions, better stability, and a simpler implementation. For these reasons, we will only consider SPC-MRI-GARK in the construction of surrogate model timestepping techniques.

An SPC-MRI-GARK method based on the “slow” Runge–Kutta method ( $\mathcal{A}^{\{s,s\}}$ ),

$\mathcal{b}^{\{\mathbf{s}\}}, c^{\{\mathbf{s}\}})$  solves (2.1) with steps of the form:

$$(2.4a) \quad Y_i = y_n + H \sum_{j=1}^{s^{\{\mathbf{s}\}}} a_{i,j}^{\{\mathbf{s}\}} f(t_n + c_j^{\{\mathbf{s}\}} H, Y_j), \quad i = 1, \dots, s^{\{\mathbf{s}\}},$$

$$(2.4b) \quad \begin{cases} v(0) = y_n, \\ v' = f^{\{\mathbf{f}\}}(t_n + \theta, v) + \sum_{j=1}^{s^{\{\mathbf{s}\}}} \gamma_j\left(\frac{\theta}{H}\right) f^{\{\mathbf{s}\}}(t_n + c_j^{\{\mathbf{s}\}} H, Y_j), \quad \text{for } \theta \in [0, H], \\ y_{n+1} = v(H). \end{cases}$$

Similar to a traditional Runge–Kutta scheme, SPC-MRI-GARK starts by computing stage values that approximate the solution at the times  $t_n + c_i^{\{\mathbf{s}\}} H$ . In this prediction step (2.4a), the fast and slow dynamics are treated together with the timestep  $H$ . The fast part of the stage values is inaccurate from this large timestep and is discarded. A single ODE (2.4b) is solved from  $t_n$  to  $t_{n+1}$  to correct the fast dynamics and produce the next step  $y_{n+1}$ . Like MRI-GARK, there are time-dependent, polynomial forcing terms for the slow tendencies. Following [39, Definition 2.2], the definitions of  $\gamma_i(t)$ ,  $\tilde{\gamma}_i(t)$ ,  $\bar{\gamma}_i$  are identical to (2.3), except they are vector quantities with a single subscript index. While base methods of any structure are admitted in the SPC-MRI-GARK framework, only diagonally implicit methods were considered in [39]. As the focus of this paper is explicit methods, we have derived new explicit methods of orders two and three and present their coefficients in Appendix A.

**3. Method formulation.** Following the process outlined in the introduction, we seek to apply the MRI-GARK method (2.2) to the partitioned problem (1.4) in order to construct a solution process that can incorporate surrogate model information. We start with the modified fast ODE (2.2b):

$$(3.1) \quad \begin{aligned} v'_i(\theta) &= \Delta c_i^{\{\mathbf{s}\}} \mathbf{V} f_{\text{sur}}(T_i + \Delta c_i^{\{\mathbf{s}\}} \theta, \mathbf{W}^* v_i(\theta)) \\ &+ \sum_{j=1}^{i+1} \gamma_{i,j}\left(\frac{\theta}{H}\right) (f(T_j, Y_j) - \mathbf{V} f_{\text{sur}}(T_j, \mathbf{W}^* Y_j)). \end{aligned}$$

In (3.1), the full model  $f$  only appears in the forcing terms, and for explicit methods, it is evaluated at previously computed stage values. Only the surrogate model  $f_{\text{sur}}$  needs to be evaluated at each of the infinitesimal steps to compute  $v_i(H)$ .

Note that in formulation (3.1),  $v_i \in \mathbb{C}^N$  evolves in the full space, and there is no benefit from choosing a surrogate model that evolves in a lower dimensional space. To resolve this, we first split  $v_i$  into the parts residing inside and outside the surrogate model space:

$$v_i(\theta) = \mathbf{V} \mathbf{W}^* v_i(\theta) + (\mathbf{I}_{N \times N} - \mathbf{V} \mathbf{W}^*) v_i(\theta).$$

More formally,  $\mathbf{V} \mathbf{W}^*$  and  $(\mathbf{I}_{N \times N} - \mathbf{V} \mathbf{W}^*)$  define oblique projections onto the range of  $\mathbf{V}$  and the nullspace of  $\mathbf{W}^*$ , respectively. We now consider the solution to (3.1) from the perspective of these two, complementary subspaces.

Starting outside the surrogate model space, we have that

$$\begin{aligned}
 (\mathbf{I}_{N \times N} - \mathbf{V}\mathbf{W}^*) v_i(H) &= (\mathbf{I}_{N \times N} - \mathbf{V}\mathbf{W}^*) \left( Y_i + \int_0^H v'_i(\theta) d\theta \right) \\
 (3.2) \qquad \qquad \qquad &= (\mathbf{I}_{N \times N} - \mathbf{V}\mathbf{W}^*) \left( Y_i + H \sum_{j=1}^i \bar{\gamma}_{i,j} f(T_j, Y_j) \right),
 \end{aligned}$$

where we have used (2.3) and the fact that  $(\mathbf{I}_{N \times N} - \mathbf{V}\mathbf{W}^*) \mathbf{V} = \mathbf{0}_{N \times S}$  by (1.3). Equation (3.2) reveals that inside the nullspace of  $\mathbf{W}^*$  the solution equation (3.1) becomes a Runge–Kutta stage. Therefore, we exclude the components in this subspace during the infinitesimal step integration of (3.1).

We now consider the dynamics (3.1) projected onto the surrogate model space:

$$\begin{aligned}
 z_i(\theta) &:= \mathbf{W}^* v_i(\theta) \in \mathbb{C}^S, \\
 (3.3) \qquad z'_i(\theta) &= \Delta c_i^{\{s\}} f_{\text{sur}}(T_i + \Delta c_i^{\{s\}} \theta, z_i(\theta)) \\
 &\quad + \sum_{j=1}^{i+1} \gamma_{i,j} \left( \frac{\theta}{H} \right) (\mathbf{W}^* f(T_j, Y_j) - f_{\text{sur}}(T_j, \mathbf{W}^* Y_j)).
 \end{aligned}$$

The solution to (3.1) can be expressed as the sum of its two components:

$$v_i(H) = \mathbf{V} z_i(H) + (\mathbf{I}_{N \times N} - \mathbf{V}\mathbf{W}^*) \left( Y_i + H \sum_{j=1}^{i+1} \bar{\gamma}_{i,j} f(T_j, Y_j) \right).$$

Thus to compute an MRI-GARK stage, we only need to solve an ODE of dimension  $S$  instead of  $N$ . We summarize the simplifications of (2.2) in Definition 3.1 and provide a graphical illustration in Figure 1.

**DEFINITION 3.1 (SM-MRI-GARK).** *A surrogate model MRI-GARK (SM-MRI-GARK) method solves the ODE (1.1) with the help of the surrogate model (1.2) using steps of the form*

$$(3.4a) \quad Y_1 = y_n,$$

$$(3.4b) \quad \left\{ \begin{aligned} &z_i(0) = \mathbf{W}^* Y_i, \\ &T_i = t_n + c_i^{\{s\}} H, \\ &z'_i(\theta) = \Delta c_i^{\{s\}} f_{\text{sur}}(T_i + \Delta c_i^{\{s\}} \theta, z_i(\theta)) \\ &\quad + \sum_{j=1}^{i+1} \gamma_{i,j} \left( \frac{\theta}{H} \right) (\mathbf{W}^* f(T_j, Y_j) - f_{\text{sur}}(T_j, \mathbf{W}^* Y_j)), \quad \text{for } \theta \in [0, H], \\ &Y_{i+1} = \mathbf{V} z_i(H) + (\mathbf{I}_{d \times d} - \mathbf{V}\mathbf{W}^*) \left( Y_i + H \sum_{j=1}^{i+1} \bar{\gamma}_{i,j} f(T_j, Y_j) \right), \\ &i = 1, \dots, s^{\{s\}}, \end{aligned} \right.$$

$$(3.4c) \quad y_{n+1} = Y_{s^{\{s\}}+1}.$$

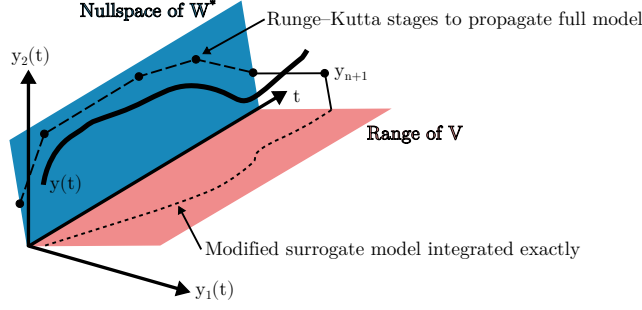


Fig. 1: Illustration of SM-MRI-GARK for a two-variable ODE and a surrogate model that evolves in a one-dimensional subspace.

*Remark 3.2* (SM-MRI-GARK for hierarchical surrogate models). For certain applications an entire hierarchy of surrogate models  $f, f_{\text{sur}}^{[1]}, f_{\text{sur}}^{[2]}, \dots, f_{\text{sur}}^{[m]}$  may be available. In such scenarios, one can take advantage of all models by applying SM-MRI-GARK recursively. First, the highest fidelity models  $f$  and  $f_{\text{sur}}^{[1]}$  are applied to (3.4). The ODE (3.4b), is then solved using an SM-MRI-GARK method with  $\Delta c_i^{\{s\}} f_{\text{sur}}^{[2]}$  as the surrogate model. Its ODEs are solved using an SM-MRI-GARK method with  $\Delta c_i^{\{s\} \times 2} f_{\text{sur}}^{[3]}$  as the surrogate model. This is continued until we reach  $\Delta c_i^{\{s\} \times (m-1)} f_{\text{sur}}^{[m]}$  as the lowest fidelity surrogate model. Note the power of  $\Delta c_i^{\{s\}}$  scaling the surrogate models can be eliminated by applying the change of variable  $\theta \rightarrow \theta / \Delta c_i^{\{s\}}$  to (3.4b).

*Remark 3.3* (Connection to EPRIRK-K methods). In [42], Sandu showed that exponential Runge–Kutta methods are special case of MRI-GARK methods when the linear-nonlinear partitioning

$$y' = \underbrace{\mathbf{L} y}_{f^{\{l\}}(t,y)} + \underbrace{f(t,y) - \mathbf{L} y}_{f^{\{s\}}(t,y)}$$

is used. Conversely, MRI-GARK can be viewed as a generalization of exponential Runge–Kutta methods where the piece integrated exactly can be linear or nonlinear.

An analogous connection can be made between EPIRK-K [29] and SM-MRI-GARK. EPIRK-K is an extension of exponential propagation iterative methods of Runge-Kutta type (EPIRK) [50] that approximates the Jacobian  $\mathbf{J}_n = f_y(t_n, y_n)$  appearing in matrix exponentials and related matrix functions with a Krylov-subspace approximation  $\mathbf{U}\mathbf{U}^* \mathbf{J}_n \mathbf{U}\mathbf{U}^*$ . SM-MRI-GARK with  $\mathbf{V} = \mathbf{W} = \mathbf{U}$  and  $f_{\text{sur}}(t, y_{\text{sur}}) = \mathbf{U}^* \mathbf{J}_n \mathbf{U} y_{\text{sur}}$  recovers the full class of EPIRK-K schemes.

As a simple example of an SM-MRI-GARK method, consider forward Euler as the base method and the internally consistent [42, Section 3.1.1] coupling  $\gamma_{1,1}(t) = 1$ :

$$\begin{aligned} z(0) &= \mathbf{W}^* y_n \\ (3.5) \quad z'(\theta) &= f_{\text{sur}}(t_n + \theta, z(\theta)) + \mathbf{W}^* f(t_n, y_n) - f_{\text{sur}}(t_n, \mathbf{W}^* y_n), \quad \text{for } \theta \in [0, H], \\ y_{n+1} &= \mathbf{V} z(H) + (\mathbf{I}_{d \times d} - \mathbf{V}\mathbf{W}^*) (y_n + H f(t_n, y_n)). \end{aligned}$$

Equation (3.5) is only first order accurate; however, second and third order SM-MRI-GARK schemes can be constructed using the coefficients provided in Appendix A. In

order to implement these efficiently, we have provided pseudocode in [Algorithm 3.1](#). It minimizes the number of full and surrogate model evaluations, as well as the number of matrix-vector products involving  $\mathbf{V}$  and  $\mathbf{W}^*$ .

---

**Algorithm 3.1** Pseudocode for explicit SM-MRI-GARK [\(3.4\)](#).

---

```

1: procedure SM-MRI-GARK( $f, f_{\text{sur}}, \mathbf{V}, \mathbf{W}^*, t_0, t_{\text{end}}, y_0, N_{\text{steps}}$ )
2:    $y = y_0$ 
3:    $\hat{y} = \mathbf{W}^* y_0$ 
4:    $H = (t_{\text{end}} - t_0) / N_{\text{steps}}$ 
5:   for  $n = 1, \dots, N_{\text{steps}}$  do
6:     for  $i = 1, \dots, s^{\{\mathbf{s}\}}$  do
7:        $T_i = t_0 + (n + c_i^{\{\mathbf{s}\}})H$ 
8:        $k_i = f(T_i, y)$ 
9:        $\hat{k}_i = \mathbf{W}^* k_i$ 
10:       $\hat{\ell}_i = \hat{k}_i - f_{\text{sur}}(T_i, \hat{y})$ 
11:       $\hat{w} = \hat{y} + H \sum_{j=1}^i \bar{\gamma}_{i,j} \hat{k}_j$ 
12:       $y = y + H \sum_{j=1}^i \bar{\gamma}_{i,j} k_j$ 
13:       $\hat{y} = \text{OdeSolve} \left( \begin{array}{l} z'_i(\theta) = \Delta c_i^{\{\mathbf{s}\}} f_{\text{sur}}(T_i + \Delta c_i^{\{\mathbf{s}\}} \theta, z_i(\theta)) + \sum_{j=1}^i \gamma_{i,j}(\frac{\theta}{H}) \hat{\ell}_j, \\ \text{timespan} = [0, H], \text{initial\_condition} = \hat{y} \end{array} \right)$ 
14:       $y = y + \mathbf{V}(\hat{y} - \hat{w})$ 
15:     end for
16:   end for
17:   return  $y$ 
18: end procedure

```

---

**3.1. Formulation for SPC-MRI-GARK.** A similar process can be used to apply SPC-MRI-GARK [\(2.4\)](#) to the ODE [\(1.4\)](#). For brevity, we avoid replicating the simplifications [\(3.2\)](#) and [\(3.3\)](#) and directly present the method formulation in the following definition.

**DEFINITION 3.4** (SM-SPC-MRI-GARK). *A surrogate model SPC-MRI-GARK (SM-SPC-MRI-GARK) method solves the ODE [\(1.1\)](#) with the help of the surrogate model [\(1.2\)](#) using steps of the form*

$$(3.6a) \quad Y_i = y_n + H \sum_{j=1}^{s^{\{\mathbf{s}\}}} a_{i,j}^{\{\mathbf{s}\}} f(t_n + c_j^{\{\mathbf{s}\}} H, Y_j), \quad i = 1, \dots, s^{\{\mathbf{s}\}},$$

$$(3.6b) \quad \left\{ \begin{array}{l} z(0) = \mathbf{W}^* y_n, \\ z(\theta)' = f_{\text{sur}}(t_n + \theta, z(\theta)) \\ \quad + \sum_{j=1}^{s^{\{\mathbf{s}\}}} \gamma_j(\frac{\theta}{H}) \left( \mathbf{W}^* f(t_n + c_j^{\{\mathbf{s}\}} H, Y_j) - f_{\text{sur}}(t_n + c_j^{\{\mathbf{s}\}} H, \mathbf{W}^* Y_j) \right), \\ \text{for } \theta \in [0, H], \\ y_{n+1} = \mathbf{V} z(H) + (\mathbf{I}_{d \times d} - \mathbf{V} \mathbf{W}^*) \left( y_n + H \sum_{j=1}^{s^{\{\mathbf{s}\}}} b_j f(t_n + c_j^{\{\mathbf{s}\}} H, Y_j) \right). \end{array} \right.$$



The SM-MRI-GARK Euler method from (3.5) also happens to be an SM-SPC-MRI-GARK method. The base method is again forward Euler, and the coupling is  $\gamma_1(t) = 1$ . Methods with more than one stage will not coincide, however, as SM-SPC-MRI-GARK has one modified fast ODE per step while SM-MRI-GARK has  $s^{\{s\}}$ . Another distinction, which can be seen in Algorithm 3.2, is that SM-SPC-MRI-GARK only requires one matrix-vector product with  $\mathbf{V}$  per step, while SM-MRI-GARK requires  $s^{\{s\}}$ .

---

**Algorithm 3.2** Pseudocode for explicit SM-SPC-MRI-GARK (3.6).

---

```

1: procedure SM-SPC-MRI-GARK( $f, f_{\text{sur}}, \mathbf{V}, \mathbf{W}^*, t_0, t_{\text{end}}, y_0, N_{\text{steps}}$ )
2:    $y = y_0$ 
3:    $\hat{y} = \mathbf{W}^* y_0$ 
4:    $H = (t_{\text{end}} - t_0) / N_{\text{steps}}$ 
5:   for  $n = 1, \dots, N_{\text{steps}}$  do
6:      $t_n = t_0 + nH$ 
7:     for  $i = 1, \dots, s^{\{s\}}$  do
8:        $k_i = f(t_n + c_i^{\{s\}}H, y + H \sum_{j=1}^{i-1} a_{i,j}^{\{s\}} k_j)$ 
9:        $\hat{k}_i = \mathbf{W}^* k_i$ 
10:       $\hat{\ell}_i = \hat{k}_i - f_{\text{sur}}(t_n + c_i^{\{s\}}H, \hat{y} + H \sum_{j=1}^{i-1} a_{i,j}^{\{s\}} \hat{k}_j)$ 
11:    end for
12:     $\hat{w} = \hat{y} + H \sum_{j=1}^{s^{\{s\}}} b_j^{\{s\}} \hat{k}_j$ 
13:     $y = y + H \sum_{j=1}^{s^{\{s\}}} b_j^{\{s\}} k_j$ 
14:     $\hat{y} = \text{OdeSolve}\left(z'(\theta) = f_{\text{sur}}(t_n + \theta, z(\theta)) + \sum_{j=1}^{s^{\{s\}}} \gamma_j\left(\frac{\theta}{H}\right) \hat{\ell}_j, \right.$ 
        $\left. \text{timespan} = [0, H], \text{initial\_condition} = \hat{y}\right)$ 
15:     $y = y + \mathbf{V}(\hat{y} - \hat{w})$ 
16:  end for
17:  return  $y$ 
18: end procedure

```

---

**4. Error analysis.** Consider the edge case where the surrogate model is taken to be the full model and  $\mathbf{V} = \mathbf{W}^* = \mathbf{I}_{N \times N}$ . The stages of (3.4) simplify to

$$\begin{aligned}
Y_1 &= y_n, \\
\begin{cases} z_i(0) = Y_i, \\ z'_i = \Delta c_i^{\{s\}} f_{\text{sur}}(t_n + c_i^{\{s\}}H + \Delta c_i^{\{s\}}\theta, z_i), \\ Y_{i+1} = z_i(H), \end{cases} & \quad \text{for } \theta \in [0, H], \\
y_{n+1} &= Y_{s^{\{s\}}+1}.
\end{aligned}$$

This is simply the original ODE (1.1) solved between the abscissae of a Runge–Kutta method. With the infinitesimal step assumption, the error is zero. At the other extreme, take the surrogate model to be  $f_{\text{sur}}(t, y_{\text{sur}}) = 0_N$ . Again, (3.4) can be

$$Y_1 = y_n,$$

$$Y_{i+1} = Y_i + H \sum_{j=1}^i \bar{\gamma}_{i,j} f(t_n + c_i^{\{s\}} H, Y_j), \quad i = 1, \dots, s^{\{s\}},$$

$$y_{n+1} = Y_{s^{\{s\}}+1}.$$

While neither of these two choices for the surrogate model are particularly interesting, they illustrate how the accuracy of SM-MRI-GARK and SM-SPC-MRI-GARK depends on several factors including the accuracy of the surrogate model, the projection matrices  $\mathbf{V}$  and  $\mathbf{W}$ , and the method coefficients. In this section, we analyze the structure of local truncation error

$$(4.1) \quad \text{LTE}_{n+1} = y(t_{n+1}) - y_{n+1} = C H^{p+1} + \mathcal{O}(H^{p+2})$$

The new families of methods in this paper are derived as special cases of MRI-GARK and SPC-MRI-GARK. Interestingly, it is also possible to view MRI-GARK and SPC-MRI-GARK as special cases of the surrogate model methods. When

$$\mathbf{V} = \mathbf{W}^* = \mathbf{I}_{N \times N}, \quad f(t, y) = f^{\{\mathbf{f}\}}(t, y) + f^{\{\mathbf{s}\}}(t, y), \quad f_{\text{sur}}(t, y) = f^{\{\mathbf{f}\}}(t, y),$$

We now discuss the leading error constant  $C$  in (4.1). N-Trees provide an elegant way to quantify the terms of which it is composed. For our multirate methods, there are two partitions, so we use the set of two-trees  $\mathbb{T}_2$ . Tree vertices are “colored” either fast (black circle) or slow (white circle). Let  $\mathbb{T}_2^{\{\text{f}\}}$  be the set of trees in  $\mathbb{T}_2$  with all vertices fast-colored (including the empty tree), and  $\mathbb{T}_2 \setminus \mathbb{T}_2^{\{\text{f}\}}$  the set of trees with at least one slow-colored node. We have that

$$(4.2) \quad C = \sum_{\substack{\mathbf{u} \in \mathbb{T}_2 \setminus \mathbb{T}_2^{\{\mathbf{f}\}} \\ \rho(\mathbf{u}) = p+1}} \frac{1}{\sigma(\mathbf{u})} \left( \Phi(\mathbf{u}) - \frac{1}{\gamma(\mathbf{u})} \right) F(\mathbf{u})(y),$$

[illegible]

where  $\rho(\mathbf{u})$ ,  $\sigma(\mathbf{u})$ ,  $\gamma(\mathbf{u})$ , are the order, symmetries, and density, respectively [5]. The elementary weight  $\Phi(\mathbf{u})$  depends only on the method and its coefficients. For  $\mathbf{u} \in \mathbb{T}_2^{\{\mathbf{f}\}}$ ,

$\Phi(\mathbf{u}) = 1/\gamma(\mathbf{u})$  by the infinitesimal step assumption, which allows us to exclude this subset of trees from the summation in (4.2). Finally, the elementary differentials have the recursive, tensorial definition:

$$(4.3a) \quad F(\emptyset)(y) = y,$$

$$(4.3b) \quad F(\bullet)(y) = \mathbf{V}f_{\text{sur}}(\mathbf{W}^*y),$$

$$(4.3c) \quad F(\circ)(y) = f(y) - \mathbf{V}f_{\text{sur}}(\mathbf{W}^*y),$$

$$(4.3d)$$

$$F([u_1, \dots, u_m]^{\{\mathbf{f}\}})(y) = \mathbf{V}f_{\text{sur}}^{(m)}(\mathbf{W}^*y)(\mathbf{W}^*F(u_1)(y), \dots, \mathbf{W}^*F(u_m)(y)),$$

$$(4.3e)$$

$$F([u_1, \dots, u_m]^{\{\mathbf{s}\}})(y) = f^{(m)}(y)(F(u_1)(y), \dots, F(u_m)(y)) - F([u_1, \dots, u_m]^{\{\mathbf{f}\}})(y).$$

A tree  $\mathbf{u} \in \mathbb{T}_2$  can be expressed as  $[u_1, \dots, u_m]^{\{\sigma\}}$  where  $\sigma$  is the color of the root vertex and  $u_1, \dots, u_m$  are the nonempty subtrees left when the root is removed. Table 1 provides examples of terms appearing in (4.2).




$\mathbf{u}$	$F(\mathbf{u})(y)$	$\rho(\mathbf{u})$	$\sigma(\mathbf{u})$	$\gamma(\mathbf{u})$
	$f(y) - \mathbf{V}f_{\text{sur}}(\mathbf{W}^*y)$	1	1	1
	$f'(y)\mathbf{V}f_{\text{sur}}(\mathbf{W}^*y) - \mathbf{V}f'_{\text{sur}}(\mathbf{W}^*y)f_{\text{sur}}(\mathbf{W}^*y)$	2	1	2
	$f''(y)(f(y), f(y)) - f''(y)(f(y), \mathbf{V}f_{\text{sur}}(\mathbf{W}^*y))$	3	1	3

Table 1: Examples of trees, elementary differentials, and other tree properties.

Using (4.2), the local truncation error of SM-MRI-GARK Euler from (3.5) is

$$\text{LTE}_{n+1}^{\text{Euler}} = \frac{1}{2}(f'(y_n) - \mathbf{V}f'_{\text{sur}}(\mathbf{W}^*y_n)\mathbf{W}^*)f(y_n)H^2 + \mathcal{O}(H^3).$$

Note that each tree in the summation in (4.2) contains at least one slow node. From (4.3e), a slow-colored vertex corresponds to the surrogate model error or one of its derivatives appearing in an elementary differential. In order to quantify the error in the surrogate model, suppose there exists a (small) constant  $\varepsilon$  such that:

$$\|f(y_n) - \mathbf{V}f_{\text{sur}}(\mathbf{W}^*y_n)\| \leq \varepsilon,$$

$$\left\| f^{(m)}(y_n)(x_1, \dots, x_m) - \mathbf{V}f_{\text{sur}}^{(m)}(\mathbf{W}^*y_n)(\mathbf{W}^*x_1, \dots, \mathbf{W}^*x_m) \right\| \leq \varepsilon \|x_1\| \cdots \|x_m\|,$$

for  $m = 1, \dots, p$ . Here  $\|\cdot\|$  denotes an arbitrary norm on  $\mathbb{C}^N$ . This yields the bounds

$$\|F(\bullet)(y_n)\| \leq d_0 + \varepsilon, \quad \left\| F([u_1, \dots, u_m]^{\{\mathbf{f}\}})(y_n) \right\| \leq (d_m + \varepsilon) \prod_{i=1}^m \|F(u_i)(y_n)\|,$$

$$\|F(\circ)(y_n)\| \leq \varepsilon, \quad \left\| F([u_1, \dots, u_m]^{\{\mathbf{s}\}})(y_n) \right\| \leq \varepsilon \prod_{i=1}^m \|F(u_i)(y_n)\|,$$

where  $d_0 = \|f(y_n)\|$  and  $d_m$  is the operator norm of  $f^{(m)}(y_n)$ . Now we have that

$$\|C\| \leq \sum_{\substack{\mathbf{u} \in \mathbb{T}_2 \setminus \mathbb{T}_2^{\{\mathbf{f}\}} \\ \rho(\mathbf{u})=p+1}} \left| \frac{1}{\sigma(\mathbf{u})} \left( \Phi(\mathbf{u}) - \frac{1}{\gamma(\mathbf{u})} \right) \right| \varepsilon^{\rho^{\{\mathbf{s}\}}(\mathbf{u})} \left( \varepsilon + \max_{i=0, \dots, p} d_i \right)^{\rho^{\{\mathbf{f}\}}(\mathbf{u})} = \sum_{i=1}^{p+1} c_i \varepsilon^i,$$

where  $\rho^{\{\sigma\}}(\mathbf{u})$  is the number of  $\sigma$ -colored vertices in  $\mathbf{u}$ . The constants  $c_i$  only depend on  $f$  and the order condition residuals; they are independent of  $f_{\text{sur}}$ ,  $\mathbf{V}$ ,  $\mathbf{W}$ ,  $H$  and  $\epsilon$ . As we might expect, the local truncation error decreases as the accuracy of the surrogate model and its derivatives increase.

### 5. Construction of surrogate models for accelerating time integration.

This sections discusses several techniques to construct a surrogate model  $f_{\text{sur}}$  and the associated linear operators  $\mathbf{V}$  and  $\mathbf{W}^*$ , with a computationally favorable balance of accuracy and evaluation cost.

**5.1. Reduced-order models (ROMs).** There are numerous techniques from the reduced-order modeling community that may be used to generate the surrogate models including proper orthogonal decomposition (POD) [48], Krylov-subspace methods [20], reduced basis methods [31], discrete empirical interpolation method [10], and dynamic mode decomposition [46, 49]. Other multi-resolution methods based on Fourier or wavelet transformation [7] could be used to only capture coarse information about the model.

**5.2. Multimesh models.** Consider a numerical approach to discretize a partial differential equation (PDE) in space over a computational mesh using, for example, the finite element, difference, or volume method. A surrogate model can come from solving the PDE on a coarser mesh or using a lower order spatial discretization. This provides an approximation to capture the “shape” of the solution that is cheaper and also enjoys a less strict Courant–Friedrichs–Lewy (CFL) condition. If the meshes are nested,  $\mathbf{W}$  is a subset of columns of the identity matrix, and  $\mathbf{V}$  is a sparse interpolation matrix. We note that this strategy closely resembles multigrid methods [53]. The relaxation and prolongation operators, however, have to be chosen such as  $\mathbf{W}^*\mathbf{V} = \mathbf{I}_{N \times N}$ , such as the 1D relaxation stencil  $\begin{bmatrix} 0 & 1 & 0 \end{bmatrix}$  and the 1D prolongation stencil  $\begin{bmatrix} 1/2 & 1 & 1/2 \end{bmatrix}$ .

**5.3. Applying simplifying approximations to the full model.** By linearizing, filtering, averaging, simply ignoring, or otherwise approximating certain terms in  $f$ , a computationally inexpensive  $f_{\text{sur}}$  can be produced. In [9, Section 6], for example, a surrogate model of z-level ocean model is produced by a vertical averaging of barotropic velocities. Consider also a direct N-body simulation with a Barnes-Hut or fast multipole method used as the surrogate model. For this example, the surrogate models happen to have the same state representation as the full model, and therefore,  $\mathbf{S} = \mathbf{N}$  and  $\mathbf{V} = \mathbf{W} = \mathbf{I}_{N \times N}$ .

**5.4. Data-driven surrogate models.** When sufficient input and output data is available, supervised learning approaches are a viable option to generate approximate models for a system. A variety of techniques have been developed, some depending on system identification and sparse dictionary learning [40], others using neural networks to discover operators and right-hand side functions [34]. Patch data, both in time and space [24] have been used to train machine learning models that can reproduce crude or partial dynamics of the full system. In some cases, the data driven dynamics reside in the full space, so  $\mathbf{S} = \mathbf{N}$  and  $\mathbf{V} = \mathbf{W} = \mathbf{I}_{N \times N}$ . In other cases, the dynamics could reside in the dominant modes of the data, in which case  $\mathbf{S} < \mathbf{N}$  and  $\mathbf{V}$  and  $\mathbf{W}$  are determined by the method.

**6. Numerical experiments.** In order to assess the convergence and performance properties of the new surrogate model time-steppers, we apply them to a set of four ODE systems using different types of surrogate models. The methods considered in the experiments are SM-MRI-GARK Euler from (3.5) and the four methods

from [Appendix A](#). We compare these with their base methods, which are traditional Runge–Kutta methods, when only the full or only the surrogate model is used. In all the experiments, the error is computed by comparing a numerical solution to a high-accuracy reference solution at the final time. The solution using only the surrogate model resides in the surrogate model subspace, so it is multiplied by  $\mathbf{V}$  before computing error.

**6.1. Quasi-geostrophic model and quadratic ROM.** The quasi-geostrophic (QG) equations [\[13, 15, 16\]](#), are a well-studied set of approximations to both atmospheric and ocean flow. The QG equations have a wide range of well-studied lower dimensional approximations. For our use case, a quadratic POD-Galerkin ROM makes an excellent surrogate model.

We follow the formulations of [\[28, 41\]](#), and the same exact setup as utilized in [\[32\]](#):

$$(6.1) \quad \begin{aligned} \omega_t + J(\psi, \omega) - \text{Ro}^{-1} \psi_x &= \text{Re}^{-1} \Delta \omega + \text{Ro}^{-1} F, \\ \omega &= -\Delta \psi, \\ J(\psi, \omega) &\equiv \psi_y \omega_x - \psi_x \omega_y. \end{aligned}$$

Here  $\omega$  represents the vorticity,  $\psi$  the streamfunction,  $\text{Re} = 450$  the Reynolds number, and  $\text{Ro} = 0.0036$  the Rossby number. The forcing term is selected to be a symmetric double Gyre to simulate flow in the ocean [\[28, 41\]](#):

$$F = \sin(\pi(y - 1)).$$

The domain for the problem is  $\Omega = [0, 1] \times [0, 2]$ . Homogeneous Dirichlet,

$$\psi(x, y) = 0, \quad \forall (x, y) \in \partial\Omega,$$

boundary conditions are used for all time.

For the spatial discretization, a second order finite difference is performed, with the canonical Arakawa approximation [\[4\]](#) performed on the Jacobian term,  $J$ . The domain is discretized using 63 points in the  $x$  direction and 127 points in the  $y$  direction. The discretization begets the discrete stream function variable  $\psi$ . The relation between the streamfunction and vorticity is used to define the time derivative of the streamfunction variable  $\psi_t$ , which we will take as the PDE of interest.

Following [\[28\]](#), and using the method of snapshots [\[48\]](#), we construct basis transformation operators that capture the time-averaged dominant linear modes of the system. The basis transformations are represented by the orthogonal, in  $L^2$ , linear operators  $\mathbf{V}$ , and  $\mathbf{W}^*$ , where  $y_{\text{sur}} = \mathbf{W}^* \psi$  represents the basis transformation from streamfunction space into ROM space. Details as to how these are derived are found in [\[32\]](#).

In order to construct a reduced-order model we have to optimally approximate the time derivative of the reduced-order state. As [\(6.1\)](#) is quadratic in nature, we can construct a quadratic POD-Galerkin reduced-order model, of the form

$$y'_{\text{sur}} = f_{\text{sur}}(y_{\text{sur}}) = \mathbf{W}^* f(\mathbf{V} y_{\text{sur}}) = b + \mathbf{A} y_{\text{sur}} + y_{\text{sur}}^T \mathbf{B} y_{\text{sur}},$$

where  $y_{\text{sur}}$  is the state in the POD basis,  $f$  is the solution to the Poisson equation in [\(6.1\)](#) for the streamfunction derivative  $\psi_t$ ,  $b \in \mathbb{R}^S$  corresponds to the forcing term  $\text{Ro}^{-1} F$ ,  $\mathbf{A} \in \mathbb{R}^{S \times S}$  corresponds to the linear term  $\text{Ro}^{-1} \psi_x + \text{Re}^{-1} \Delta \omega$ , and  $\mathbf{B} \in \mathbb{R}^{S \times S \times S}$  corresponds to the Jacobian term  $-J(\psi, \omega)$ . We take  $S$ , the dimension of the reduced-order state space  $y_{\text{sur}}$  to be significantly smaller than the dimension of the space of

the discretized streamfunction,  $N$ . It is known from [32] that for this specific spatial discretization, utilizing  $N = 8001$  points,  $S = 40$  modes corresponds to 98.1% of the total kinetic energy of the system, while  $S = 80$  modes corresponds to 99.4% of the total energy, meaning that this problem should be extremely well-suited to dimensional reduction.

The timespan for which we run the system is a ten day forecast, which for the given parameters is approximately 0.109. The ROM was built in the interpolatory regime on the test timespan using 2000 evenly-spaced snapshots. The model and the reduced-order model implementations for the experiments have been taken from [38].

Figure 2 shows the convergence of the QG equations with respect to a ROM. We have not plotted the results of the Runge–Kutta methods using only the surrogate model as they produced errors orders of magnitude larger than the other methods. For a fixed number of timesteps, SM-MRI-GARK and SM-SPC-MRI-GARK consistently have less error than Runge–Kutta methods using only the full model. At order three, however, the more accurate ROM of size  $S = 80$  is needed to achieve a substantial decrease in error.

**6.2. Lorenz ’96 with a machine learning surrogate model.** The Lorenz ’96 problem [27] is given by

$$(6.2) \quad \frac{d}{dt}X_k = -X_{k-2}X_{k-1} + X_{k-1}X_{k+1} - X_k + F, \quad k = 1, 2, \dots, 40,$$

with periodic boundary conditions, and a forcing term  $F = 8$ . Due to its chaotic dynamics, this problem is prominently used in data assimilation and atmospheric research. Readers interested in current literature on machine learning surrogate models based on Lorenz ’96 may refer to [17, 36].

In the following experiments, a neural network model with fully-connected layers was trained to approximate the right-hand side function in (6.2). Therefore the projections are  $\mathbf{V} = \mathbf{W}^* = \mathbf{I}_{d \times d}$  and the trained network acts as  $f_{\text{sur}}$ . The network consists of input and output layers and a hidden layer of dimension 80. The input and hidden layers use the softplus activation function while the output layer does not have any activations.

Similar to [27], the initial condition  $X_{20}(0) = 8.008$  and  $X_i(0) = 8$  for  $i \neq 20$  is propagated for 2 units of time to expel transient effects and the developed solution is used as the true initial condition. The training data is taken from 5000 equally-spaced solutions of the full model within the interval  $t \in [2, 10]$  and, the convergence tests are performed over timespan  $t \in [4, 8]$ .

The results are shown in Figure 3. We note that merely integrating the surrogate model did not produce a stable solution in any of the experiments. On the other hand, when used together with the full model in SM-MRI-GARK and SM-SPC-MRI-GARK methods, the accuracy of the solution increases significantly compared to the full model solution.

**6.3. Brusselator PDE.** The test problem BRUS from [23, Section II.10] is based on the Brusselator reaction-diffusion PDE

$$(6.3) \quad \begin{aligned} \frac{\partial u}{\partial t} &= \alpha \nabla^2 u + 1 + u^2 v - 4.4u, \\ \frac{\partial v}{\partial t} &= \alpha \nabla^2 v + 3.4u - u^2 v, \end{aligned}$$

where  $\alpha = 0.002$ . The spatial domain is the unit square  $0 \leq x, y \leq 1$  with zero, Neumann boundary conditions for both  $u$  and  $v$ . Using the method of lines, this

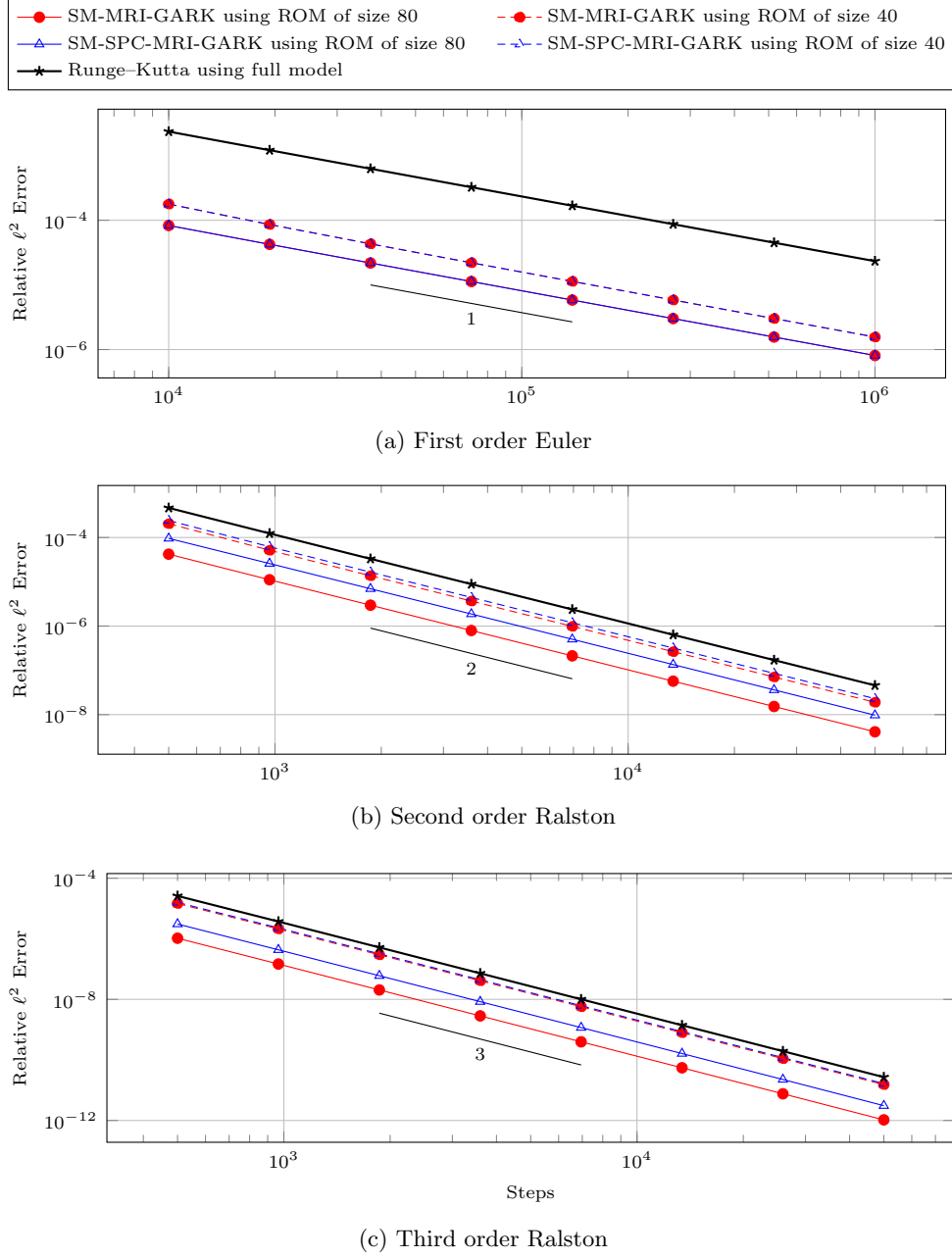


Fig. 2: Convergence plots for the Quasi-Geostrophic equations (6.1).

is discretized with second order central finite difference on a uniform  $P \times P$  grid. Starting at the initial conditions

$$u(t = 0, x, y) = 0.5 + y, \quad v(t = 0, x, y) = 1 + 5x,$$

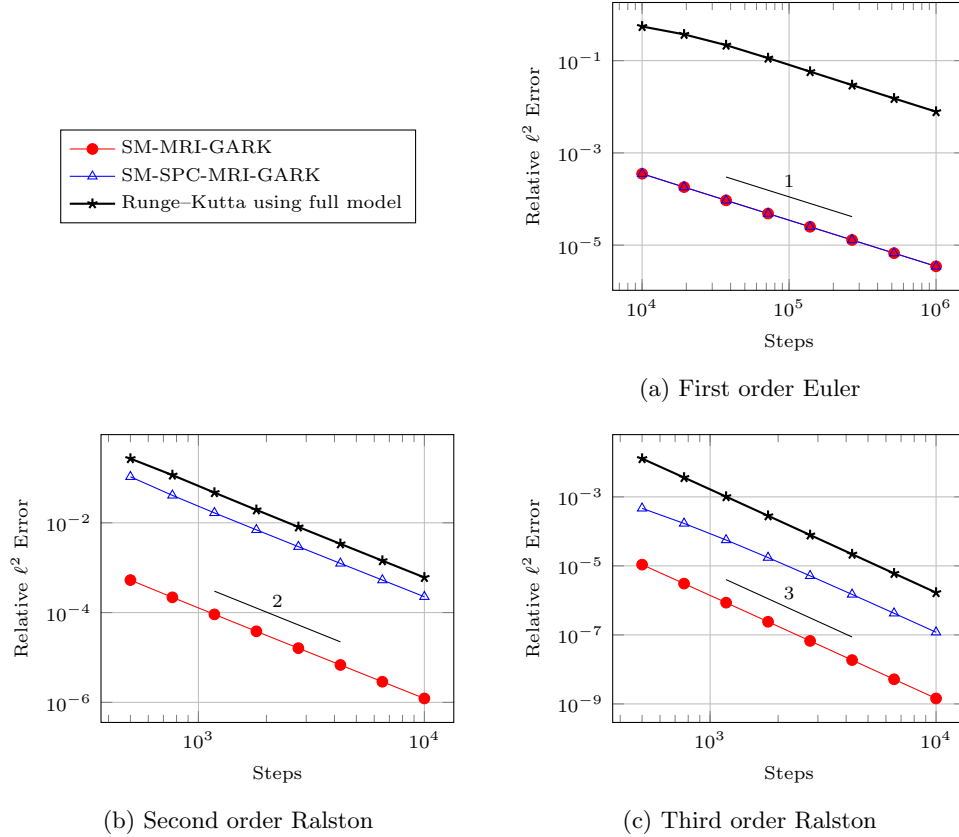


Fig. 3: Convergence plots for the Lorenz '96 problem (6.2).

we seek the solution at  $t = 7.5$ .

In our experiments,  $P = 257$ , and thus,  $N = 2P^2 = 132098$ . For the surrogate model, we take the approach described in subsection 5.2 where we use the same finite difference discretization of (6.3) but on a coarser mesh. In particular, coarse meshes of size  $P = 129$  and  $P = 65$  are used, which nest inside the fine mesh. The modified fast ODEs (3.4b) and (3.6b) are solved with *one* step of a Runge-Kutta method one or two orders higher than the base method. We found that this uses the fewest evaluations of  $f_{\text{sur}}$  while keeping the ODE solution errors negligible.

Comparing the performance of the integrators is our primary goal with the Brusselator problem, and we implemented the tests in C. For each integrator and surrogate model size, the runtime and error was recorded for a range of eight stepsizes. The results are plotted in Figure 4. At orders one and two, SM-MRI-GARK and SM-SPC-MRI-GARK show clear speedups over Runge-Kutta solutions using only the full model. In addition, the performance increases as the surrogate model mesh becomes finer. Unfortunately, the results are reversed at order three. Profiling of the code helped to identify why SM-MRI-GARK and SM-SPC-MRI-GARK performed poorly. On a  $129 \times 129$  grid, evaluations of  $f_{\text{sur}}$  are about 25% as expensive as evaluation  $f$ . The linear operators  $\mathbf{V}$  and  $\mathbf{W}^*$  have efficient, matrix-free implementations,



but are still 75% as expensive as  $f$ . These two factors caused one step of SM-MRI-GARK and SM-SPC-MRI-GARK to take approximately twice as long as a traditional Runge–Kutta step. At order three, the reduction in error is not enough to overcome this large overhead.

**6.4. Advection PDE.** Finally, we consider the following 2D advection problem with zero, Dirichlet boundary conditions:

$$\begin{aligned}\frac{\partial u}{\partial t} + a \cdot \nabla u &= 0, & \text{on } \Omega = [0, 1] \times [0, 1], \\ u(t, x, y) &= 0, & \text{on } \partial\Omega.\end{aligned}$$

The velocity field corresponds to the Molenkamp-Crowley problem:

$$a(x, y) = \left[ 2\pi \left( y - \frac{1}{2} \right), -2\pi \left( x - \frac{1}{2} \right) \right],$$

We start with the initial condition

$$u(t = 0, x, y) = \exp(-100((x - 0.35)^2 + (y - 0.35)^2))$$

and stop at  $t = 2$ . This allows the initial profile to rotate clockwise twice about the center of the domain.

For the method of lines discretization in space, we represent  $\Omega$  with a  $P \times P$  uniform, triangular mesh and apply a nodal discontinuous Galerkin (DG) method. The order in space is chosen to match the order in time. This yields the linear ODE

$$(6.4) \quad y' = \mathbf{M}^{-1} \mathbf{K} y,$$

where  $\mathbf{M}$  and  $\mathbf{K}$  are mass and advection matrices, respectively. We use the C++ library MFEM [2] for this DG discretization, and in particular, base it on the serial version of example 9 provided in MFEM version 4.1.

Again, we try the multimesh approach by using a mesh size of  $P = 100$  for  $f$  and a mesh size of  $P = 50$  for  $f_{\text{sur}}$ . This size of the ODE (6.4) for each experiment is listed in Table 2.

Order of time and space discretization	Dimension of full model N	Dimension of surrogate model S
1	$6 \times 10^4$	$1.5 \times 10^4$
2	$1.2 \times 10^5$	$3 \times 10^4$
3	$2 \times 10^5$	$5 \times 10^4$

Table 2: Dimensions of the full and surrogate models used in the advection experiment.

In contrast to the Brusselator problem (6.3), the advection problem is linear and hyperbolic. Moreover, profiling reveals an evaluation of the RHS of (6.4) is much more expensive than an interpolation between meshes due, in part, to the linear solve with the mass matrix. Based on the discussion in the previous subsection, we may expect better performance results at order three, and indeed, that is the case.

Figure 5 shows the error and timing for the integrators over a range of eight step-sizes. All SM-MRI-GARK and SM-SPC-MRI-GARK methods outperform Runge–Kutta methods with speedups ranging from approximately 3 to 725. The error for

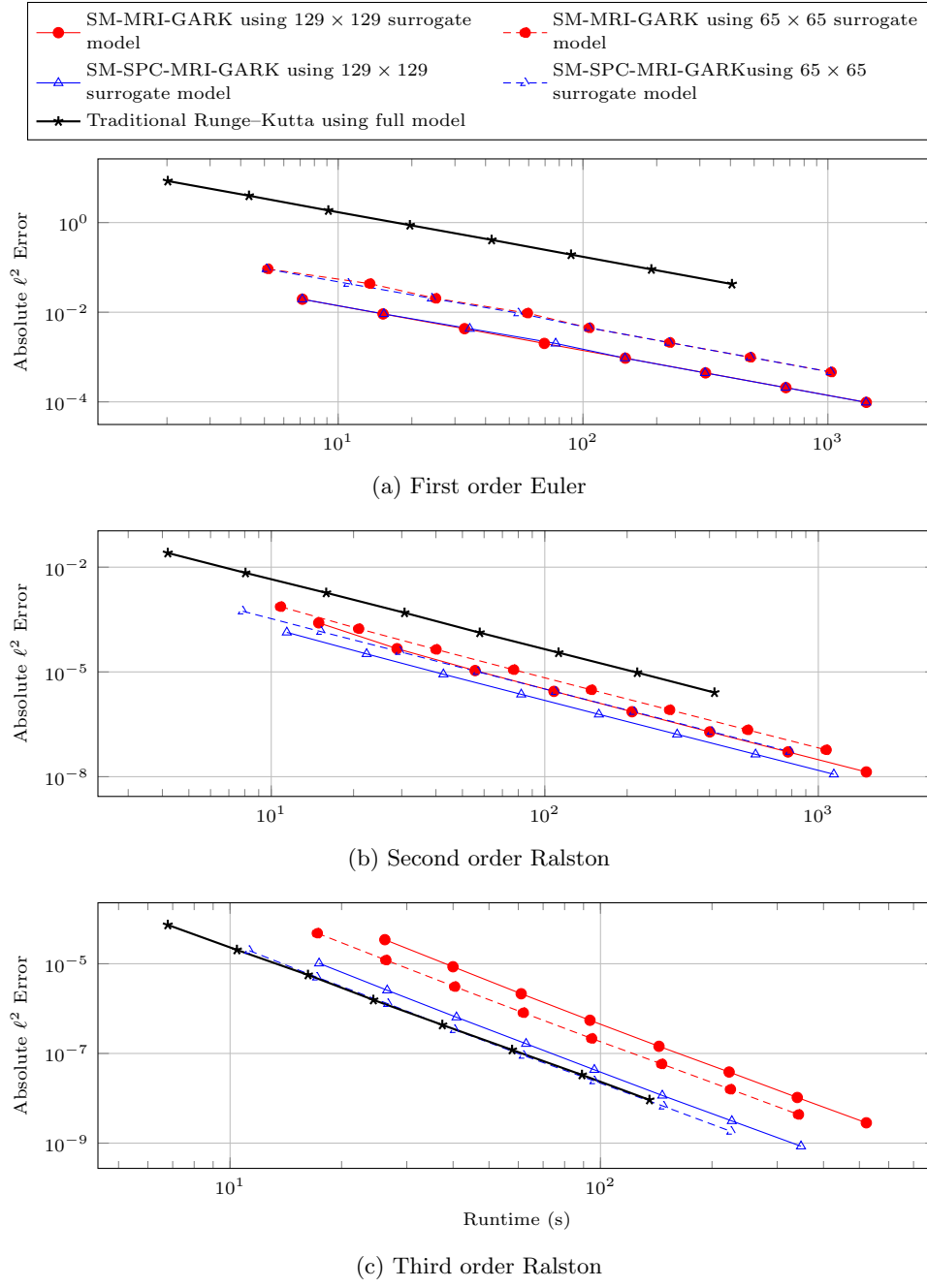


Fig. 4: Work precision diagrams for BRUS (6.3).

the Runge-Kutta methods using the surrogate model remains nearly constant, which indicates that spatial errors dominate temporal errors.

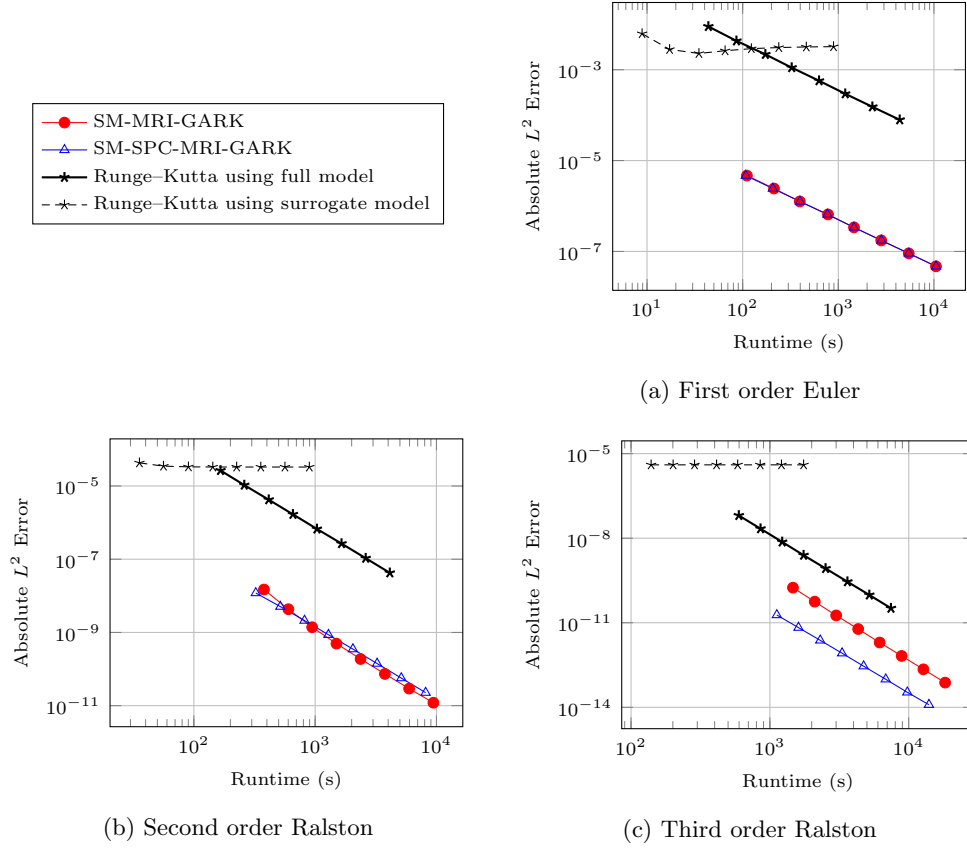


Fig. 5: Work precision diagrams for advection problem (6.4).

**7. Conclusions.** This work develops a new methodology to accelerate the time integration of large ODEs using surrogate models. Specifically, surrogate information is incorporated into the numerical solution of the original ODEs using multirate methods. We derive and analyze two implementations of this new time-stepping technique: SM-MRI-GARK and SM-SPC-MRI-GARK. Both combine continuous evolution of the surrogate model with discrete Runge-Kutta steps of the full ODE. There are numerous ways to generate surrogate models that offer flexible trade-offs between accuracy, computational cost, and stability. The new methods are designed such that the overall order of accuracy is independent of the surrogate model. The more accurate the surrogate models are, the smaller the error constants are, which leads to smaller local truncation errors of the overall integration.

Numerical experiments reveal that, at low orders of accuracy, it is possible to achieve orders of magnitude speedups over traditional Runge-Kutta methods. As the order increases, overheads associated with evaluations of  $\mathbf{V}$ ,  $\mathbf{W}^*$ , and the surrogate model are penalized more when measuring efficiency, and speedups tend to decrease. There is not a clear winner between SM-MRI-GARK and SM-SPC-MRI-GARK; their relative performance appears to depend heavily on the properties of the full and surrogate models.

While this paper focuses on explicit methods for nonstiff problems, the authors also plan to explore implicit and implicit-explicit methods [8, 52] for stiff problems and differential algebraic equations. Further extensions include applying and comparing other flavors of multirate methods for constructing surrogate model based time-steppers.

#### Appendix A. Explicit MRI-GARK and SPC-MRI-GARK methods of orders two and three.

Table 3 provides coefficients for new MRI-GARK and SPC-MRI-GARK schemes based on Ralston’s optimal second and third order Runge–Kutta methods [35]. For readers interested in using different base methods or including embedded methods, we have provided a Mathematica notebook in the supplementary materials with general, parameterized families of methods.

Order	Base Method			MRI-GARK $\Gamma(t)$	SPC-MRI-GARK $\gamma(t)$
2	0	0	0	$\begin{bmatrix} \frac{2}{3} & 0 \\ -\frac{5}{12} & \frac{3}{4} \end{bmatrix}$	$\begin{bmatrix} -\frac{1}{2} + \frac{3t}{2} \\ \frac{3}{2} - \frac{3t}{2} \end{bmatrix}$
	$\frac{2}{3}$	$\frac{2}{3}$	0		
		$\frac{1}{4}$	$\frac{3}{4}$		
3	0	0	0	$\begin{bmatrix} \frac{1}{2} & 0 & 0 \\ -\frac{11}{4} + \frac{9t}{2} & 3 - \frac{9t}{2} & 0 \\ \frac{47}{36} - \frac{13t}{6} & -\frac{1}{6} - \frac{t}{2} & -\frac{8}{9} + \frac{8t}{3} \end{bmatrix}$	$\begin{bmatrix} 1 - \frac{2t}{3} - \frac{4t^2}{3} \\ -2t + 4t^2 \\ \frac{8t}{3} - \frac{8t^2}{3} \end{bmatrix}$
	$\frac{1}{2}$	$\frac{1}{2}$	0		
	$\frac{3}{4}$	0	$\frac{3}{4}$		
		$\frac{2}{9}$	$\frac{1}{3}$		

Table 3: Second and third order MRI-GARK and SPC-MRI-GARK coefficients.

#### REFERENCES

- [1] A. ABDULLE, M. J. GROTE, AND G. R. DE SOUZA, *Stabilized explicit multirate methods for stiff differential equations*, arXiv preprint arXiv:2006.00744, (2020).
- [2] R. ANDERSON, J. ANDREJ, A. BARKER, J. BRAMWELL, J.-S. CAMIER, J. C. V. DOBREV, Y. DUDUIT, A. FISHER, T. KOLEV, W. PAZNER, M. STOWELL, V. TOMOV, I. AKKERMAN, J. DAHM, D. MEDINA, AND S. ZAMPINI, *MFEM: A modular finite element library*, Computers & Mathematics with Applications, (2020), <https://doi.org/10.1016/j.camwa.2020.06.009>.
- [3] J. ANDRUS, *Numerical solution for ordinary differential equations separated into subsystems*, SIAM Journal on Numerical Analysis, 16 (1979), pp. 605–611.
- [4] A. ARAKAWA, *Computational design for long-term numerical integration of the equations of fluid motion: Two-dimensional incompressible flow. Part I*, Journal of Computational Physics, 1 (1966), pp. 119–143.
- [5] A. L. ARAÚJO, A. MURUA, AND J. M. SANZ-SERNA, *Symplectic Methods Based on Decompositions*, SIAM Journal on Numerical Analysis, 34 (1997), pp. 1926–1947, <https://doi.org/10.1137/S0036142995292128>.
- [6] T. P. BAUER AND O. KNOTH, *Extended multirate infinitesimal step methods: Derivation of order conditions*, Journal of Computational and Applied Mathematics, (2019), <https://doi.org/10.1016/j.cam.2019.112541>.
- [7] S. L. BRUNTON AND J. N. KUTZ, *Data-driven science and engineering: Machine learning, dynamical systems, and control*, Cambridge University Press, 2019.
- [8] A. CARDONE, Z. JACKIEWICZ, A. SANDU, AND H. ZHANG, *Extrapolation-based implicit-explicit general linear methods*, Numerical Algorithms, 65 (2014), pp. 377–399, <https://doi.org/10.1007/s11075-013-9759-y>.

- [9] L. CHACÓN, G. CHEN, D. KNOLL, C. NEWMAN, H. PARK, W. TAITANO, J. WILLERT, AND G. WOMELDORFF, *Multiscale high-order/low-order (HOLO) algorithms and applications*, Journal of Computational Physics, 330 (2017), pp. 21–45, <https://doi.org/10.1016/j.jcp.2016.10.069>.
- [10] S. CHATURANTABUT AND D. C. SORESENSEN, *Nonlinear model reduction via discrete empirical interpolation*, SIAM Journal on Scientific Computing, 32 (2010), pp. 2737–2764.
- [11] E. CONSTANTINESCU AND A. SANDU, *Multirate timestepping methods for hyperbolic conservation laws*, Journal on Scientific Computing, 33 (2007), pp. 239–278, <https://doi.org/10.1007/s10915-007-9151-y>.
- [12] E. CONSTANTINESCU AND A. SANDU, *Extrapolated multirate methods for differential equations with multiple time scales*, Journal of Scientific Computing, 56 (2013), pp. 28–44, <https://doi.org/10.1007/s10915-012-9662-z>.
- [13] J. FERGUSON, *A numerical solution for the barotropic vorticity equation forced by an equatorially trapped wave*, master's thesis, University of Victoria, 2008.
- [14] A. I. FORRESTER AND A. J. KEANE, *Recent advances in surrogate-based optimization*, Progress in Aerospace Sciences, 45 (2009), pp. 50–79, <https://doi.org/10.1016/j.paerosci.2008.11.001>.
- [15] E. L. FOSTER, T. ILIESCU, AND Z. WANG, *A finite element discretization of the streamfunction formulation of the stationary quasi-geostrophic equations of the ocean*, Comput. Methods Appl. Mech. Engrg., 261 (2013), pp. 105–117.
- [16] E. L. FOSTER, T. ILIESCU, AND D. R. WELLS, *A conforming finite element discretization of the streamfunction form of the unsteady quasi-geostrophic equations*, Int. J. Numer. Anal. Mod., 13 (2016).
- [17] D. J. GAGNE, H. M. CHRISTENSEN, A. C. SUBRAMANIAN, AND A. H. MONAHAN, *Machine Learning for Stochastic Parameterization: Generative Adversarial Networks in the Lorenz '96 Model*, Journal of Advances in Modeling Earth Systems, 12 (2020), p. e2019MS001896, <https://doi.org/10.1029/2019MS001896>.
- [18] C. GEAR, *Multirate methods for ordinary differential equations*, tech. report, Illinois Univ., Urbana (USA). Dept. of Computer Science, 1974.
- [19] C. GEAR AND D. WELLS, *Multirate linear multistep methods*, BIT, 24 (1984), pp. 484–502.
- [20] E. GRIMME, *Krylov projection methods for model reduction*, theses, University of Illinois at Urbana Champaign, May 1997, <https://tel.archives-ouvertes.fr/tel-01711328>.
- [21] M. GÜNTHER AND A. SANDU, *Multirate generalized additive Runge-Kutta methods*, Numerische Mathematik, 133 (2016), pp. 497–524, <https://doi.org/10.1007/s00211-015-0756-z>.
- [22] C. HACHTEL, J. KERLER-BACK, A. BARTEL, M. GÜNTHER, AND T. STYKEL, *Multirate DAE/ODE-simulation and model order reduction for coupled field-circuit systems*, in Scientific Computing in Electrical Engineering, U. Langer, W. Amrhein, and W. Zulehner, eds., Cham, 2018, Springer International Publishing, pp. 91–100.
- [23] E. HAIRER, S. P. NØRSETT, AND G. WANNER, *Solving Ordinary Differential Equations I: Non-stiff Problems*, vol. 8 of Springer Series in Computational Mathematics, Springer-Verlag, Berlin, Heidelberg, 2nd ed., 1993, <https://doi.org/10.1007/978-3-540-78862-1>.
- [24] I. G. KEVREKIDIS, C. W. GEAR, AND G. HUMMER, *Equation-free: The computer-aided analysis of complex multiscale systems*, AIChE Journal, 50 (2004), pp. 1346–1355, <https://doi.org/10.1002/aic.10106>.
- [25] O. KNOTH AND R. WOLKE, *Implicit-explicit Runge-Kutta methods for computing atmospheric reactive flows*, Applied Numerical Mathematics, 28 (1998).
- [26] P. J. LANZKRON, D. J. ROSE, AND J. T. WILKES, *An analysis of approximate nonlinear elimination*, SIAM Journal on Scientific Computing, 17 (1996), pp. 538–559, <https://doi.org/10.1137/S106482759325154X>.
- [27] E. N. LORENZ, *Predictability: A problem partly solved*, in Proc. Seminar on predictability, vol. 1, 1996.
- [28] C. MOU, H. LIU, D. R. WELLS, AND T. ILIESCU, *Data-driven correction reduced order models for the quasi-geostrophic equations: a numerical investigation*, International Journal of Computational Fluid Dynamics, 34 (2020), pp. 147–159, <https://doi.org/10.1080/10618562.2020.1723556>.
- [29] M. NARAYANAMURTHI, P. TRANQUILLI, A. SANDU, AND M. TOKMAN, *EPIRK-W and EPIRK-K time integration methods*, Journal of Scientific Computing, 78 (2019), pp. 167–201, <https://doi.org/10.1007/s10915-018-0761-3>.
- [30] Y. S. ONG, P. B. NAIR, AND A. J. KEANE, *Evolutionary optimization of computationally expensive problems via surrogate modeling*, AIAA Journal, 41 (2003), pp. 687–696, <https://doi.org/10.2514/2.1999>.
- [31] J. S. PETERSON, *The reduced basis method for incompressible viscous flow calculations*, SIAM

- Journal on Scientific and Statistical Computing, 10 (1989), pp. 777–786.
- [32] A. POPOV, C. MOU, A. SANDU, AND T. ILIESCU, *A multifidelity ensemble Kalman filter with reduced order control variates*, SIAM Journal of Scientific Computing, CSL-TR-20-2 (2020), <https://arxiv.org/abs/2007.00793>.
  - [33] N. V. QUEIPO, R. T. HAFTKA, W. SHYY, T. GOEL, R. VAIDYANATHAN, AND P. KEVIN TUCKER, *Surrogate-based analysis and optimization*, Progress in Aerospace Sciences, 41 (2005), pp. 1 – 28, <https://doi.org/10.1016/j.paerosci.2005.02.001>.
  - [34] M. RAISSI, P. PERDIKARIS, AND G. E. KARNIADAKIS, *Physics-informed neural networks: A deep learning framework for solving forward and inverse problems involving nonlinear partial differential equations*, Journal of Computational Physics, 378 (2019), pp. 686–707, <https://doi.org/10.1016/j.jcp.2018.10.045>.
  - [35] A. RALSTON, *Runge–Kutta methods with minimum error bounds*, Mathematics of computation, 16 (1962), pp. 431–437.
  - [36] S. RASP, *Coupled online learning as a way to tackle instabilities and biases in neural network parameterizations: general algorithms and Lorenz 96 case study (v1.0)*, Geoscientific Model Development, 13 (2020), pp. 2185–2196, <https://doi.org/10.5194/gmd-13-2185-2020>.
  - [37] J. RICE, *Split Runge-Kutta methods for simultaneous equations*, Journal of Research of the National Institute of Standards and Technology, 60 (1960).
  - [38] S. ROBERTS, A. A. POPOV, AND A. SANDU, *ODE test problems: a Matlab suite of initial value problems*, Tech. Report CSL-TR-19-1, Computational Science Laboratory, Virginia Tech, 2019, <https://github.com/ComputationalScienceLaboratory/ODE-Test-Problems>, <https://arxiv.org/abs/1901.04098>.
  - [39] S. ROBERTS, A. SARSHAR, AND A. SANDU, *Coupled multirate infinitesimal GARK methods for stiff differential equations with multiple time scales*, SIAM Journal on Scientific Computing, 42 (2020), pp. A1609–A1638, <https://doi.org/10.1137/19M1266952>.
  - [40] S. H. RUDY, S. L. BRUNTON, J. L. PROCTOR, AND J. N. KUTZ, *Data-driven discovery of partial differential equations*, Science Advances, 3 (2017), p. e1602614, <https://doi.org/10.1126/sciadv.1602614>.
  - [41] O. SAN AND T. ILIESCU, *A stabilized proper orthogonal decomposition reduced-order model for large scale quasigeostrophic ocean circulation*, Advances in Computational Mathematics, 41 (2015), pp. 1289–1319.
  - [42] A. SANDU, *A class of multirate infinitesimal GARK methods*, SIAM Journal on Numerical Analysis, 57 (2019), pp. 2300–2327, <https://doi.org/10.1137/18M1205492>.
  - [43] A. SANDU AND E. CONSTANTINESCU, *Multirate Adams methods for hyperbolic equations*, Journal of Scientific Computing, 38 (2009), pp. 229–249, <https://doi.org/10.1007/s10915-008-9235-3>.
  - [44] A. SARSHAR, S. ROBERTS, AND A. SANDU, *Design of high-order decoupled multirate GARK schemes*, SIAM Journal on Scientific Computing, 41 (2019), pp. A816–A847, <https://doi.org/10.1137/18M1182875>.
  - [45] M. SCHLEGEL, O. KNOTH, M. ARNOLD, AND R. WOLKE, *Multirate Runge-Kutta schemes for advection equations*, Journal of Computational and Applied Mathematics, 226 (2009), pp. 345–357.
  - [46] P. J. SCHMID, *Dynamic mode decomposition of numerical and experimental data*, Journal of fluid mechanics, 656 (2010), pp. 5–28.
  - [47] J. M. SEXTON AND D. R. REYNOLDS, *Relaxed multirate infinitesimal step methods for initial-value problems*, arXiv preprint arXiv:1808.03718, (2018).
  - [48] L. SIROVICH, *Turbulence and the dynamics of coherent structures part I: Coherent structures*, Quarterly of applied mathematics, 45 (1987), pp. 561–571.
  - [49] G. TISSOT, L. CORDIER, N. BENARD, AND B. R. NOACK, *Model reduction using dynamic mode decomposition*, Comptes Rendus Mécanique, 342 (2014), pp. 410–416.
  - [50] M. TOKMAN, *A new class of exponential propagation iterative methods of Runge–Kutta type (EPIRK)*, Journal of Computational Physics, 230 (2011), pp. 8762–8778.
  - [51] J. WENSCH, O. KNOTH, AND A. GALANT, *Multirate infinitesimal step methods for atmospheric flow simulation*, BIT Numerical Mathematics, 49 (2009), pp. 449–473.
  - [52] E. ZHAROVSKY, A. SANDU, AND H. ZHANG, *A class of IMEX two-step Runge-Kutta methods*, SIAM Journal on Numerical Analysis, 53 (2015), pp. 321–341, <https://doi.org/10.1137/130937883>.
  - [53] H. B. ZUBAIR, *Efficient Multigrid Methods based on Improved Coarse Grid Correction Techniques.*, PhD thesis, Delft University of Technology, Netherlands, 2009.